 doi:10.20944/preprints202205.0286.v1

Article

In Vivo Analysis of the Immune Response to Strontium- and Copper-doped Bioglasses

Said Alkildani [1], Armando Mandlule [1], Milena Radenković[3], Stevo Najman[3,4], Sanja Stojanović[3,4], Ole Jung [5], Yanru Ren [1,6], Baoyi Cai [1,6], Oliver Görke[6], Franziska Schmidt [6,†], and Mike Barbeck[2,†,*]

[1] BerlinAnalytix GmbH, 12109 Berlin, Germany; said.alkildani@berlinanalytix.com
[2] Department of Ceramic Materials, Institute for Materials Science and Technologies, Technical University of Berlin, 10623 Berlin, Germany; mike.barbeck@tu-berlin.de
[3] Department for Cell and Tissue Engineering, Faculty of Medicine, University of Niš, 18000 Niš, Serbia; milena1390nis@gmail.com; stevo.najman@gmail.com; s.sanja88@gmail.com
[4] Department of Biology and Human Genetics, Faculty of Medicine, University of Niš, 18000 Niš, Serbia
[5] Clinic and Policlinic for Dermatology and Venereology, University Medical Center Rostock, 18057 Rostock, Germany; ole.tiberius.jung@gmail.com
[6] Department of Prosthodontics, Geriatric Dentistry and Craniomandibular Disorders, Charité-Universitätsmedizin Berlin, corporate member of Freie Universität Berlin, Humboldt-Universität zu Berlin, and Berlin Institute of Health, 14197 Berlin, Germany.

* Correspondence: mike.barbeck@tu-berlin.de; Tel.: +49-176-81022467
† These authors contributed equally.

Abstract: Bioglasses are highly adoptable bone substitute materials, which can be combined with so-called therapeutic ions. These ions have shown to influence underlying molecular processes of the bone regeneration cascade. Moreover, it is known that bone substitutes induce an immune reaction within their implantation area involving macrophages and their pro- and anti-inflammatory subtypes dependent on their chemical composition. However, only poor knowledge exists regarding the influence of therapeutic ions onto the immune reactions and the associated bone healing. Thus, the aim of this work was to investigate the influence of strontium- and copper-doped bioglasses on the induction of M1- and M2-macrophages as well as the implant bed vascularization. **(2) Methods:** For this study, two alkali glasses were produced on basis of ICIE-16 bioglass via the melt-quench route with the addition of 5 wt% copper or strontium (ICIE16-Cu and ICIE16-Sr). Pure ICIE16 and 45S5 bioglasses were used as control materials. The bioactivity (ion release), chemical composition and the surface pattern were investigated, as well as an *in vivo* experiment was performed using the subcutaneous implantation model in rats. **(3) Results:** SEM imaging showed different formations of hydroxyapatite on the surfaces of the bioglass systems after submersion in simulated body fluid. EDX analysis confirmed the doping process by showing the release kinetics. Copper-doped bioglass exhibited a higher ion release than strontium-doped bioglass. Copper induced both a low immune cell migration and triggered a low number of M1- and M2-macrophages but also of blood vessels. The strontium-containing bioactive glass induced higher numbers of M1-macrophages after 30 days. Both copper- and strontium-doped bioglasses induced comparable numbers of M2-macrophages as found in the control groups. **(4) Conclusions:** Bioglass doping with copper and strontium did not exhibit significant influence on the foreign body response or the implantation bed vascularization *in vivo*. However, the prepared bioglass systems seemed to be biocompatible.

Keywords: bioglass; ion release; hydroxyapatite deposition; bone tissue regeneration; macrophages; vascularization; copper doping; strontium doping; 45S5; ICIE16

 doi:10.20944/preprints202205.0286.v1

1. Introduction

In the group of biomaterials, bone substitute materials (BSMs) are a small group including materials mainly based on natural or synthetic calcium phosphates and similar compounds [1]. Bioactive glass (BG) represents its own specific subgroup and has shown to be a good BSM due to its optimal bonding to newly formed bone tissue and due to the formation of a hydroxycarbonate apatite (HA) layer supporting bone regeneration [2]. Since the invention of bioactive glass materials in the 1970s by Prof. Larry L. Hench, where 45S5® Bioglass was one of the first discovered materials, a lot of research has been conducted on bioactive glasses. Silicate-based bioactive glasses and glass ceramics have been clinically used as BSMs for several decades such as Perioglas® [3] or Ceravital® [4,5]. Nevertheless, 45S5® has some disadvantages, such as the small processing window, which can lead to crystallization during the production process and thus to a reduction of bioactivity due to the presence of crystalline and amorphous phases [6,7]. Furthermore, the original composition contains a large amount of sodium to decrease the melting temperature [8], which has been shown to lead to cell death under *in vitro* conditions due to a burst release and subsequent fast increase in pH [9]. Due to the high crystallization tendency of 45S5, it is difficult to shape it into glass fibers or amorphous scaffolds without changing its initial properties and thus, the ability to bond to bone. In contrast, ICIE16 (in wt%: 48.0 SiO_2, 6.6 Na_2O, 32.9 CaO, 2.5 P_2O_5, 10.0 K_2O) was previously developed by Elgayar and coworkers [10]. It possesses a lower tendency towards crystallization and a greater sintering window [11], which makes ICIE16 a promising agent for producing various shapes including amorphous scaffolds [12].

One of the most worthwhile aspects of bioactive glasses is the ability to incorporate vast quantities of additives such as therapeutic ions (e.g., strontium, copper, zinc, or fluorine) or drugs [13]. In this context, ICIE16 is an ideal candidate for incorporation of therapeutically active ions into scaffolds, which can be used for controlled degradation [12,14]. Therapeutic ions can be added in the form of metallic ions and are also naturally present in the body. Even if they occur in the body in lower concentrations in the form of trace elements [15], higher quantities released from bioactive glasses show stimulating effects on certain cells, without being toxic [15–17]. Thus, therapeutic ions are able to enhance the biological impact of bioactive glasses and therefore, strengthen bone formation due to their stimulating effects [18]. Like any other biomaterial, bioactive glasses induce an inflammatory reaction within their implant bed [15,19]. This reaction cascade, also known as the "foreign body reaction to biomaterials", includes macrophages as central control elements, which significantly control the material-specific inflammation through the expression of a variety of signaling molecules [20]. The consensus is that the biomaterial should altogether induce an anti-inflammatory tissue response and thereby also a predominance of M2 macrophages, in order to optimally support tissue regeneration [21]. So far it is known that the strontium-addition leads to stimulation of osteoblast and reduction of osteoclast activity [18,22]. Its inclusion induces new bone formation and is therefore widely used as a therapeutic ion for osteoporosis [23]. Furthermore, copper is mainly known for the promotion of angiogenesis and (related) stimulation of bone regeneration [24,25]. However, it is completely unknown what influence these so-called therapeutic ions have on inflammatory tissue reactions that are to be strongly connected with tissue regeneration [15,18]. Thus, it was supposed that their inclusion can be used to control the material-triggered healing process by regulating the induction of M2-macrophages. In this context, it was shown that copper, zinc, and silver have anti-inflammatory and antimicrobial properties [26]. The use of therapeutic ions in dental applications, could therefore provide a lot of advantages compared to both purely inorganic bone substitute materials and also to organic biomolecules (e.g., growth factors) such as the lack of risk of decomposition or the possibility to be processed at typical manufacturing conditions [27]. Altogether, it is assumable that the addition of therapeutic ions to bioactive glasses might lead to a better bone healing process by adaption of the associated and underlying inflammatory reactions.

Thus, the aim of this work was to investigate the influence of the release of strontium and copper ions from bioactive glass-based BSM on the induction of the induction of M1- and M2-macrophage subtypes.

 doi:10.20944/preprints202205.0286.v1

Thus, the objectives of the present study were: (a) The synthesis of bioactive glass of the system 45S5 (in wt%: 45 SiO2, 24.5 CaO, 24.5 Na2O, and 6.0 P2O5) and ICIE16 (in wt%: 48.0 SiO2, 6.6 Na2O, 32.9 CaO, 2.5 P2O5, 10.0 K2O); (b) incorporation of 5 mol % strontium- or copper-ions into ICIE16; (c) examination of the influence of strontium and copper on the resulting structure and material properties; (d) evaluation of the influence of strontium and copper on the bioactivity of the synthesized glasses and the ability to form a hydroxycarbonate apatite (HA) layer; (e) assessment of the alignment of inflammation induced by ICIE16 and the strontium and copper doped glasses after the subcutaneous implantation for 10 and 30 days using previously established and published methodologies [28,29]. Thereby, both pure ICIE16 and 45S5 bioglass implants served as control materials. 45S5 Bioglass was used as a control group, due to its proven biocompatibility in literature [13].

2. Experimental Section

2.1 Materials

Four different BG alkali systems were synthesized by melt quenching, including 45S5, ICIE16 and Cu and Sr doped ICIE16, ICIE16-Cu and ICIE16-Sr, respectively. 45S5 and ICIE16 were prepared as control groups. Compared to 45S5, ICIE16 shows low crystallization tendency during sintering and remains amorphous up to 700 °C [30]. The following table provides the molecular composition of each BG group (Table 1).

Table 1. Nominal composition of the investigated BG groups (mol%).

	SiO_2	P_2O_5	Na_2O	CaO	K_2O	CuO	SrO
Control Materials							
45S5	46.1	2.6	24.4	26.9	0	0	0
ICIE16	49.46	1.07	6.6	36.27	6.6	0	0
Test Materials							
ICIE16-Cu	46.99	1.02	6.27	34.46	6.27	5	0
ICIE16-Sr	46.99	1.02	6.27	34.46	6.27	0	5

Per batch, 100 g of BG were prepared via a melt-quench process. High-purity powders (SiO2, Na2CO, Ca5HO13P3, Ca(OH)2, K2CO3, CuCO3, and SrCO3) were weighted according to their relative ratios, dried at 100 °C for 24 hours, melted at 1400 °C for 2 hours, quenched at room temperature after 2 hours, dried at 100 °C overnight, milled down to 100-315 μm particle for 3 minutes via dry ball-milling, and finally pressed into pellets using pressure of 15 bar for 3 minutes. Finally, the materials underwent gamma-sterilization.

2.2 Methods

2.2.1 in vitro Characterization

Bioactivity investigation in Simulated Body Fluid (SBF)

Scanning Electron Microscopy (SEM) and Energy-dispersive X-ray Spectroscopy (EDX)

The surface morphology of the prepared BG materials were characterized with a LEO Gemini 1530 SEM (Carl Zeiss SMT GmbH, Oberkochen, Germany), before and after immersion in simulated body fluid (SBF). The SBF was prepared according to Kokubo *et al.* [31]. The bioglasses were immersed and incubated at 37 °C for 3, 7, and 14 days, in static conditions. After incubation, the samples were removed, washed with ethanol, and dried at 50 °C. The samples were then carbon- and gold-sputtered and observed at accelerating voltages of 10–20 kV. To analyze the chemical composition and level of contamination qualitatively, energy dispersive X-ray spectra (Kα line) of disc surface areas of 1x1μm2 were recorded at 10 and 20 kV in the field emission gun SEM (FE-SEM).

 doi:10.20944/preprints202205.0286.v1

Inductively Coupled Plasma Optical Emission Spectrometry (ICP-OES)

ICP-OES measurements were performed using Ultima-2 (Horiba, Kyoto, Japan) at 252.851 nm to determine the amount of ions, which dissolute from the glass samples into the Simulated Body Fluid (SBF). For each sample, three measurements were conducted (3, 7, and 14 days).

2.2.2 In Vivo study

Experimental Design

Subcutaneous implantation was performed on 32 Sprague Dawley rats that were randomly assigned to the groups according to BG type and time point (n=4 per each group and time point). The experimental animals were anesthetized via an intraperitoneal injection of ketamine [100 mg/kg of body weight] and xylazine [5 mg/kg of body weight]). A midline incision was made in the skin of the scapular region, followed by a blunt incision to create a subcutaneous pocket. 100 mg of each BG were implanted in the subcutaneous pocket under sterile conditions and the wound was stitched with nonabsorbable suture materials. The animals were sacrificed using an overdose of the anesthesia after two time points: 10 and 30 days post *implantationem*. The biomaterials were extracted with their surrounding tissue and placed in formaldehyde solution for preservation for 24 hours. Experiments were authorized by the Local Ethical Committee of the Faculty of Medicine (University of Niš, Serbia) based on the approval of the Veterinary Directorate of the Ministry of Agriculture, Forestry and Water Management of the Republic of Serbia (approval number 323-07-01762/2019-05/9; date of approval: 01 March 2019).

Histological Workup

The explants were processed with an initial dehydration through increasing ethanol concentrations and cleared in xylene. Afterwards, the explants were treated with 10% Tris-buffered ethylenediaminetetraacetic acid (EDTA) for decalcification for 2 weeks to allow the following sectioning. The explants were then embedded in paraffin. The paraffin blocks were then sectioned with a 3-5 µm thickness. Serial sections were used for histochemical staining (i.e., hematoxylin and eosin, H&E) and immunohistochemical stainings, i.e., CD11c marker for detection of M1 macrophages, a CD163 marker for detection of M2 macrophages, and against CD31 marker for detection of endothelial cells). All antibodies were obtained from abcam (Cambridge, UK). The process of immunohistochemical staining has been thoroughly described by Lindner et al. [28]. In brief, the histological sections were treated with citrate buffer and proteinase K at pH 8 for 20 min in a water bath at 96 °C, followed by equilibration using TBS-T buffer. Subsequently, the slides were prepared by H2O2 and avidin and biotin blocking solutions (Avidin/Biotin Blocking Kit, Vector Laboratories, Burlingame, CA, USA). Incubation with the respective first antibody for 30 min was conducted, followed by incubation with the secondary antibody (goat anti-rabbit IgG-B, sc-2040, 1:200, Santa Cruz Biotechnology, Shandon, CA, USA). Afterward, the avidin–biotin–peroxidase complex (ThermoFisher Scientific, Dreeich, Germany) (30 min) was applied, and counterstaining by bluing was conducted.

Histological and Histomorphometrical Analysis

Histopathological evaluation was conducted using a conventional diagnostic microscope, Axio Imager M2 (Zeiss, Oberkochen, Germany). The evaluation included the observation of state of the implantation bed and biomaterial, which includes evaluation of: granulation tissue, types of immune cells (granulocytes, lymphocytes, macrophages, and biomaterial-associated multinucleated giant cells (BMGCs), vascularization, fibrosis, hemorrhage, and necrosis. Photographs were taken using the Axiocam 506 color connected to its software ZEN Core (Zeiss, Oberkochen, Germany).

To conduct the quantitative histomorphometrical analysis, the immunohistochemically stained slides were initially digitalized using a scanning microscope (M8, PreciPoint GmbH, Munich, Germany). Afterwards, the occurrence of M1 and M2 macrophages was analyzed using a plugin on ImageJ (National Institutes of Health, New York, United States) that was developed by Lindner and colleagues [28]. This plugin allows to measure the number of stain-positive cells per mm2 and the vascularization pattern (vessels/mm2 and vascularization percent).

 doi:10.20944/preprints202205.0286.v1

2.2.4 Statistics

Quantitative data won from the histomorphometrical analysis was represented as means with standard deviation. The data was analyzed using analysis of variance (ANOVA) tool via the GraphPad Prism 9.3.1 software (GraphPad Inc., La Jolla, United States). This analysis is to determine statistical differences between the sample groups. Statistical differences were designated as significant if p-values were less than 0.05 (* $p < 0.05$), and highly significant if p-values were less than 0.01 (** $p < 0.01$), less than 0.001 (*** $p < 0.001$) or less than 0.0001 (**** $p < 0.0001$).

3. Results

3.1 Characterization

3.1.1 Energy-dispersive X-ray Spectroscopy (EDX)

The energy-dispersive x-ray spectroscopy was used to determine the qualitative chemical composition of the samples. EDX analyses revealed the presence of Si, Na, Ca, P, and O in the group of the 45S5 samples as well as of additional K in the ICIE16 group (Figure 1). Moreover, it revealed the additional presence of Cu and Sr in the ion-doped ICIE16 groups (Figure 1).

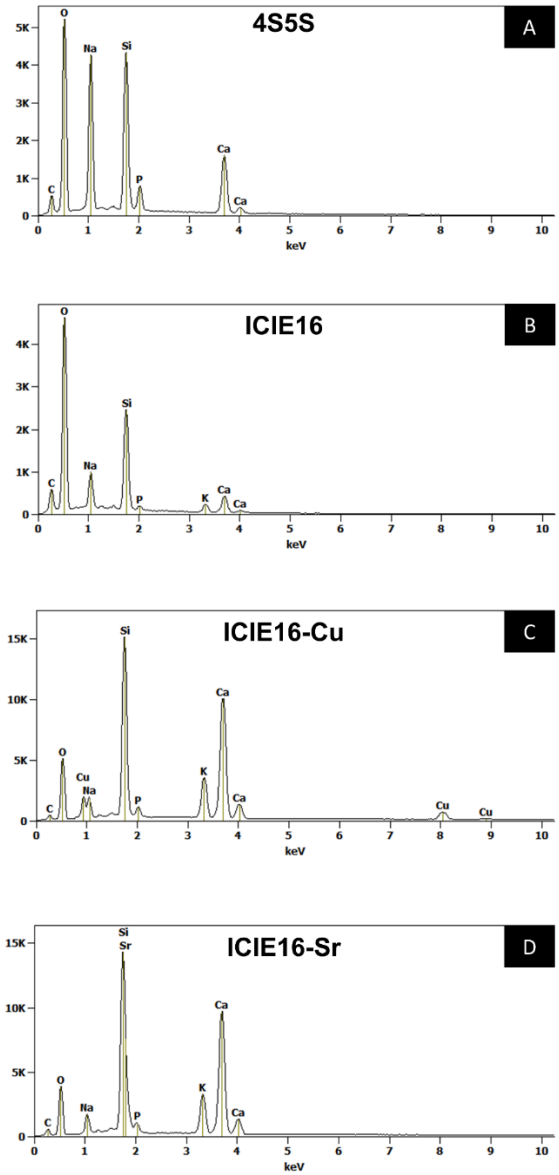

Figure 1. EDX spectra of the (A) 45S5, (B) ICIE16, (C) ICIE16-Cu and (D) ICIE16-Sr bioglass systems.

Preprints (www.preprints.org) | NOT PEER-REVIEWED | Posted: 23 May 2022 doi:10.20944/preprints202205.0286.v1

3.1.3 Inductively Coupled Plasma Optical Emission Spectrometry

The ion release of the copper- and strontium-doped materials was measured before and after immersion in SBF for 3, 7, and 14 days (Table 1 and Figure 3). The release of both ions increased with time; however, copper-doped materials showed a higher release at all time points but without significant differences.

Table 2. Release values of the therapeutic ions from bioglass (in mg/dL).

Days	Mean	SD	Mean	SD
	Cu^{2+}		Sr^{2+}	
0	0	0	0	0
3	76,79	0,31	54,27	0,33
7	97,76	0,38	65,18	0,75
14	126,17	1,04	71,32	0,43

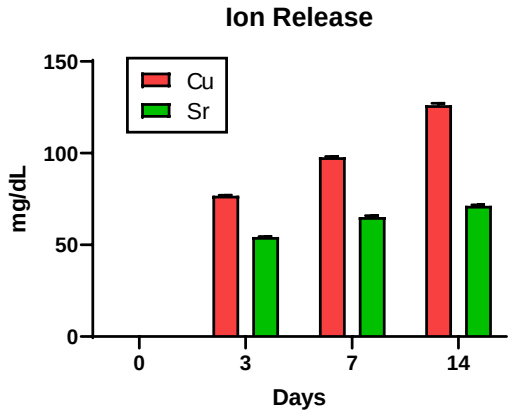

Figure 1. Cu ion release from the ion-doped ICIE16-Cu and Sr ion release from ICIE-16-Sr materials after immersion in SBF for 3, 7, and 14 days.

3.2 In Vivo

3.2.1 Histopathological Analysis

Histological analysis showed that the different BGs were detectable within the subcutaneous connective tissue at day 10 and 30 days post *implantationem*. Also, no tissue ingrowth into the BG discs has been detected. All BG samples were surrounded by inflammatory cell types, i.e., mainly macrophages beside lower numbers of granulocytes and fibroblasts at 10 days post *implantationem* (Figure 4). Furthermore, single multinucleated giant cells (BMGCs) were detectable at the materials surfaces in all study groups. The histopathological analysis revealed comparable extents of the inflammatory tissue reactions in all four study groups. However, the immunohistochemical detection revealed less macrophages within the implantation beds of the copper-doped BG and especially lower numbers of CD163-positive macrophages in this group compared to the other groups (Figure 5). Between the three other study groups no visible differences in the occurrence of CD163-positive cells were observed. Moreover, the analysis showed that also minimally lower numbers of CD11c-positive macrophages were observable in the group of the copper-doped BG compared to the other study groups that contained comparable amounts of this macrophage subtype (Figure 6). Additionally, a visible difference between the ratio of CD163- and CD11c-positive macrophages was visible in all study groups involving lower numbers of pro-inflammatory cells. Furthermore, comparative numbers of small vessels have been found within the reactive connective tissue neighbored to all implants (Figure 7).

At day 30 post *implantationem* still comparable tissue reaction patterns were detected in all BG groups. Histopathological analyses have shown that the same types of cells, i.e., mainly macrophages

Preprints (www.preprints.org) | NOT PEER-REVIEWED | Posted: 23 May 2022 doi:10.20944/preprints202205.0286.v1

as well as single granulocytes and fibroblasts were involved (Figure 4). However, the number of BMGCs at the materials surfaces was slightly increased in all groups. Additionally, the histopathological analyses revealed that the numbers of M1-macrophages have visibly increased in the groups of the strontium-doped ICIE16-Sr and the pure ICIE16 BG and their numbers were higher compared to the number of CD163-positive M2-macrophages. In contrast, in the groups of the copper-doped ICIE16-Cu and the 45S5 BG comparative numbers of both macrophage subtypes were observable (Figure 5 and Figure 6). The observation of the implantation bed vascularization showed that comparable vessel numbers were still apparent within the granulation and connective tissues surrounding all bone substitute materials (Figure 7).

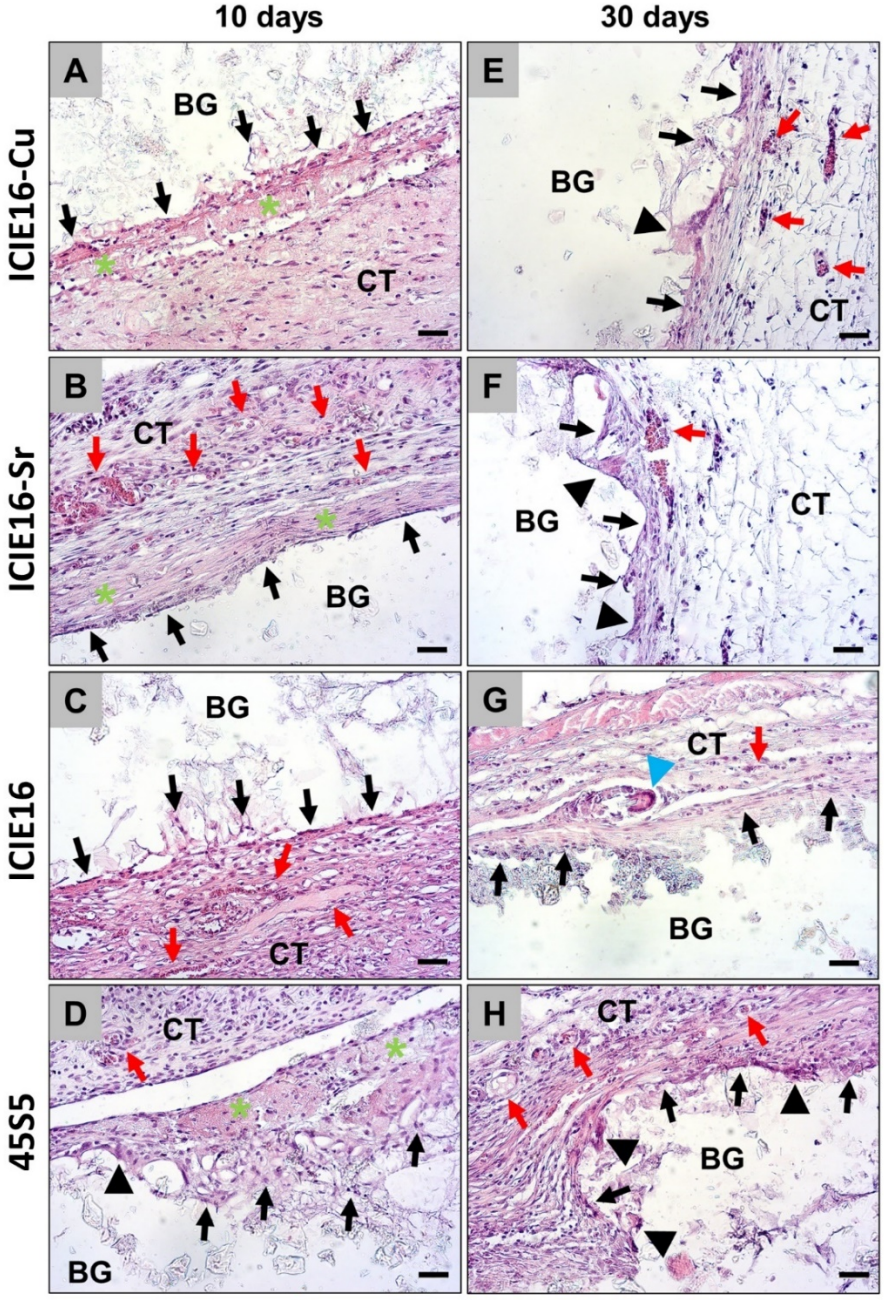

Figure 2. Exemplary histological images of the tissue reactions to the four BG compositions within the subcutaneous connective tissue (CT). Left row: tissue reactions at 10 days after implantation. Right row: tissue reactions at 30 days after implantation. Black arrows = mononuclear cells at the material tissue interfaces, black arrowheads = multinucleated cells at the material surfaces, red arrows = blood vessels, green stars = fibrin network, blue arrowhead = multinucleated giant cell associated with a fragment of the BG ICIE16 (HE staining, 20x magnifications, scalebars = 20µm).

Preprints (www.preprints.org) | NOT PEER-REVIEWED | Posted: 23 May 2022 doi:10.20944/preprints202205.0286.v1

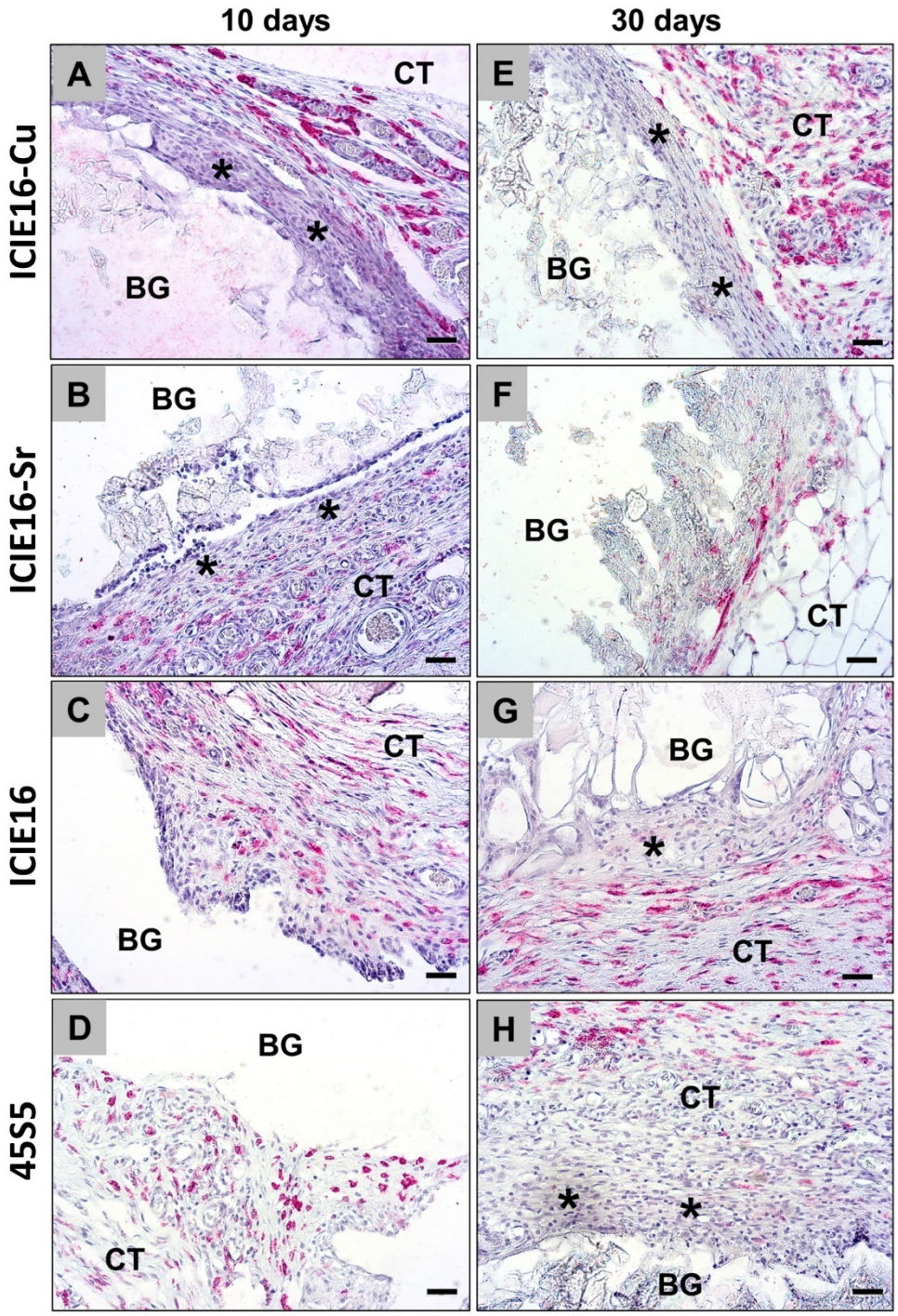

Figure 3. Exemplary histological images of the occurrence of CD163-positive M2-macrophages (red staining) within the implantation beds of the four BG compositions within the subcutaneous connective tissue (CT). Left row: 10 days after implantation. Right row: 30 days after implantation. Stars = cell walls at the material surfaces that were free of M2-macrophages (CD163-immunostainings, 20x magnifications, scalebars = 20μm).

Preprints (www.preprints.org) | NOT PEER-REVIEWED | Posted: 23 May 2022 doi:10.20944/preprints202205.0286.v1

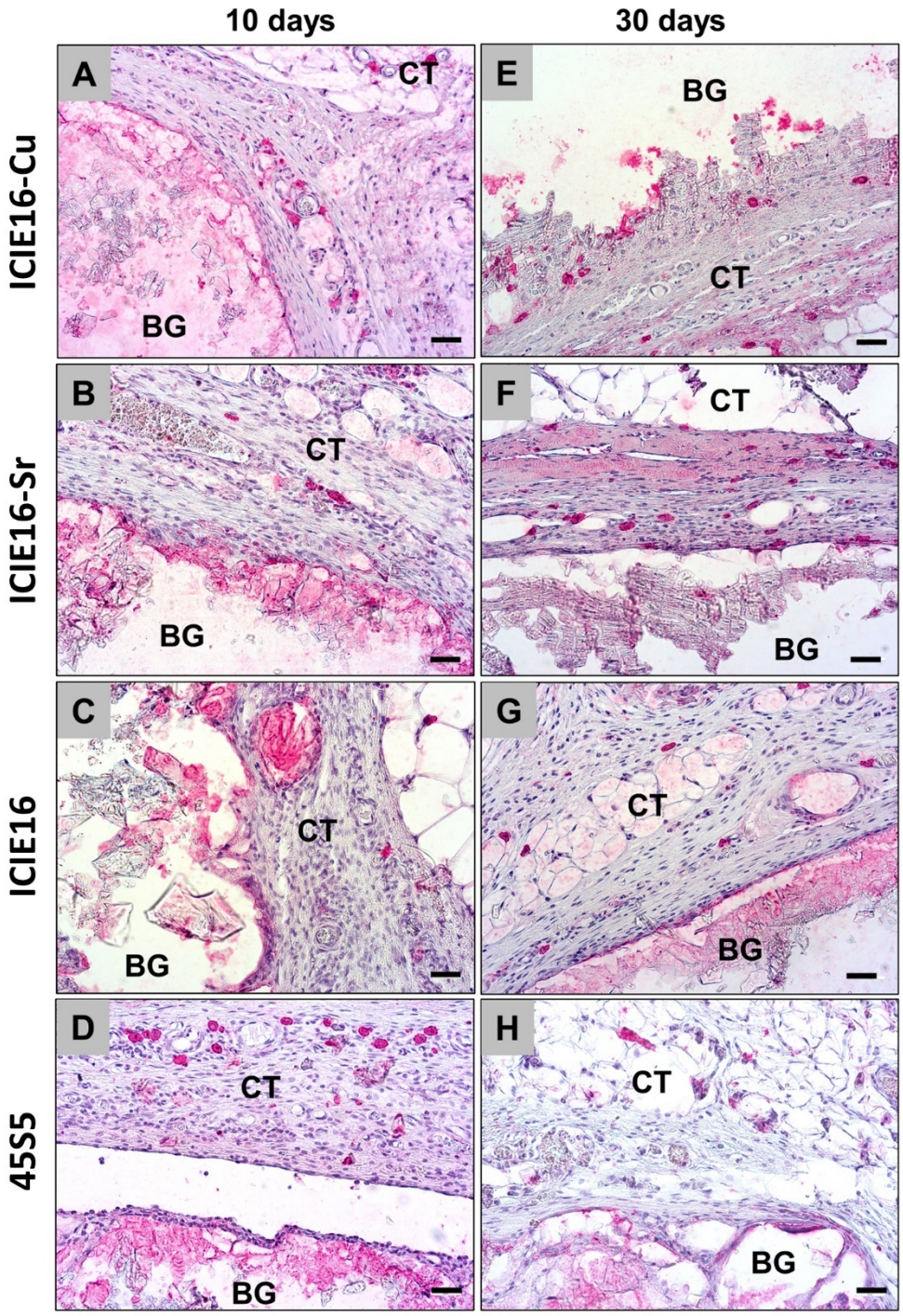

Figure 4. Exemplary histological images of the occurrence of CD11c-positive M1-macrophages (red staining) within the implantation beds of the four BG compositions within the subcutaneous connective tissue (CT). Left row: 10 days after implantation. Right row: 30 days after implantation. (CD11c-immunostainings, 20x magnifications, scalebars = 20μm).

Preprints (www.preprints.org) | NOT PEER-REVIEWED | Posted: 23 May 2022 doi:10.20944/preprints202205.0286.v1

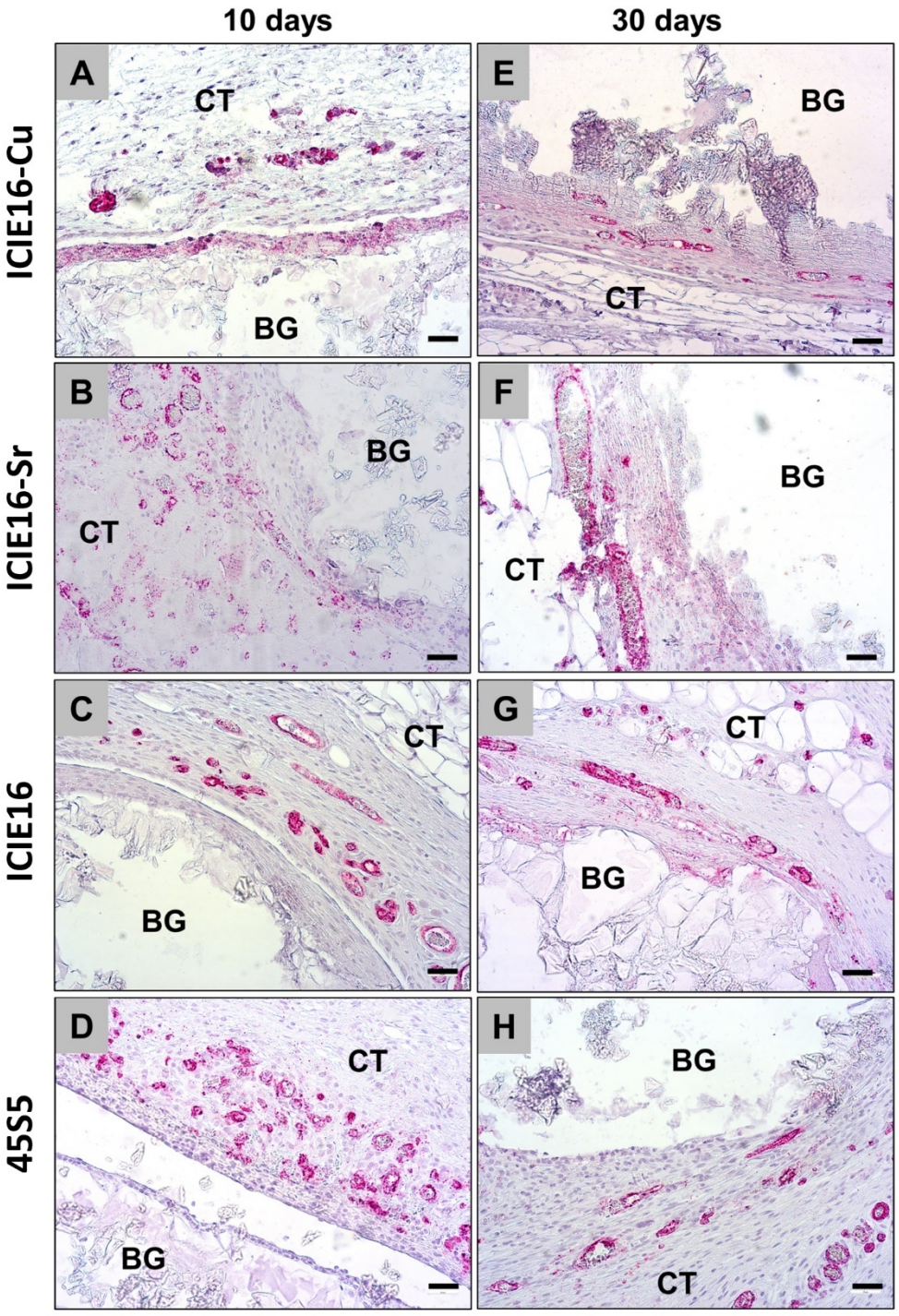

Figure 7. Exemplary histological images of the occurrence of blood vessels (red staining) within the implantation beds of the four BG compositions within the subcutaneous connective tissue (CT). Left row: 10 days after implantation. Right row: 30 days after implantation. (CD31-immunostainings, 200x magnifications, scalebars = 20µm).

3.2.2 Histomorphometrical Analysis of the Immune Response

At 10 days post *implantationem*, ICIE16-Cu induced lower numbers of pro-inflammatory M1-macrophages (612.7 ± 429.5 cells/mm2) than detected in the 45S5-group, which showed the highest values for pro-inflammatory macrophages (4167 ± 1015 cells/mm2). The evaluation furthermore revealed that in the groups of the ICIE16-Sr (2508 ± 460.3 cells/mm2) and ICIE16 (2603 ± 851.6 cells/mm2) comparable numbers of M1-macrophages were found (Figure 8). Furthermore, the

Preprints (www.preprints.org) | NOT PEER-REVIEWED | Posted: 23 May 2022 doi:10.20944/preprints202205.0286.v1

number of M1-macrophages was higher in the ICIE16-Sr-group compared to the numbers in the ICIE16-Cu-group, but only the number of M1-macrophages in the 45S5-group was significantly higher than in the ICIE16-Cu-group (**p<0.01). In the ICIE16-group (1953 ± 581.1 cells/mm2) and the 45S5-group (1529 ± 961.6 cells/mm2) highest numbers of M2-macrophages followed by the numbers in the ICIE16-Sr-group (919.1 ± 701.9 cells/mm2) and the ICIE16-Cu-group (47.73 ± 39.12 cells/mm2) were found without any significant differences.

At 30 days post *implantationem* increasing numbers of M1-macrophages were detected in the group of the ICIE16-Cu (2091 ± 1820 cells/mm2), the group of the ICIE16-Sr (4126 ± 1207 cells/mm2) and the ICIE16-group (3133 ± 1177 cells/mm2). Furthermore, the numbers of M1-macrophages in the 45S5-group decreased from 10 to 30 days (1648 ± 1278 cells/mm2).

Moreover, the number of M2-macrophages remained on a relatively low level in the group of the ICIE16-Cu (859.2 ± 380.8 cells/mm2). In the groups of the ICIE16-Sr (1350 ± 230.4 cells/mm2), the ICIE16 (1260 ± 662.2 cells/mm2) and the 45S5 (1504 ± 1401 cells/mm2) comparable higher numbers of M2-macropahges were found. Thereby, only in the latter group similar numbers of M1- and M2-macrophages were detected.

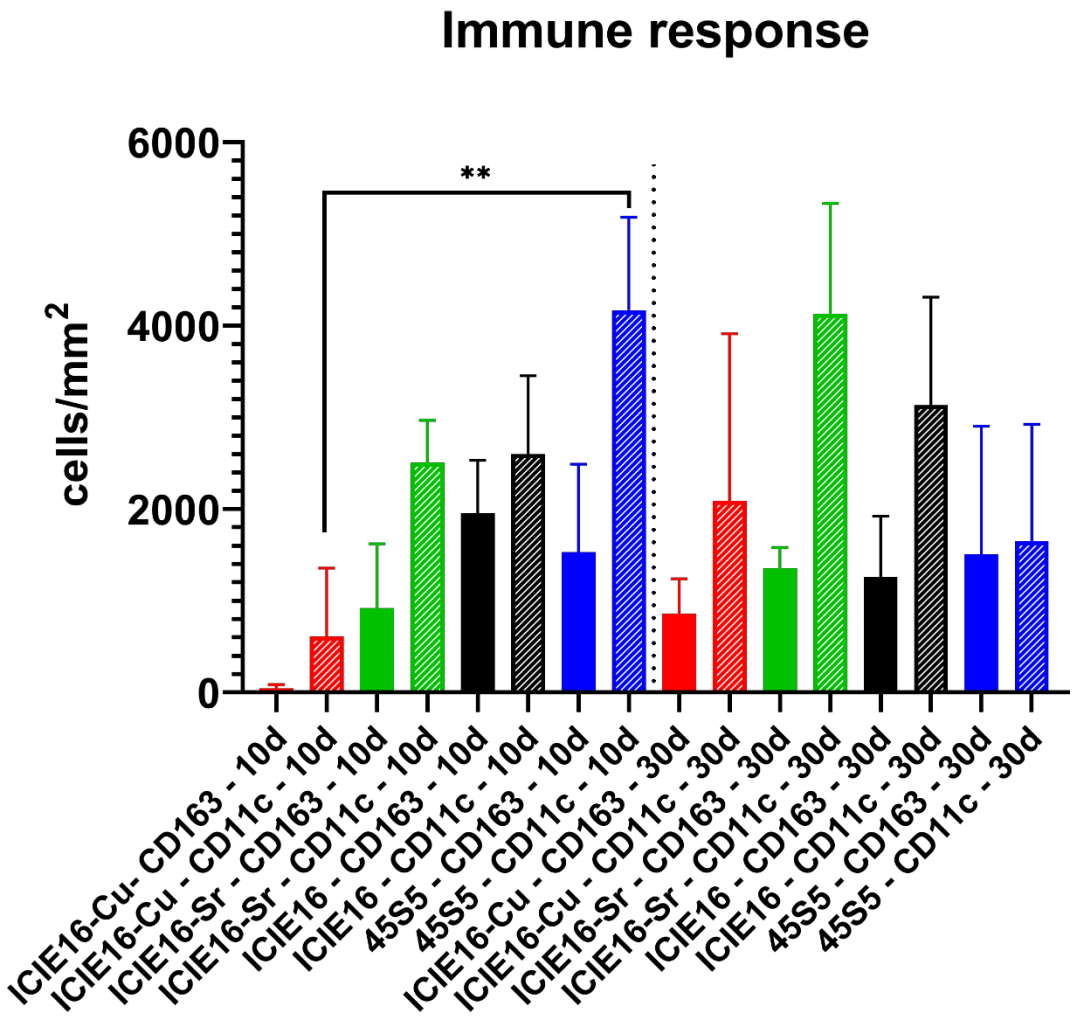

Figure 5. Results of the histomorphometrical analysis of the occurrence of CD11c-positive M1- and CD163-positive M2-macrophages (**p<0.01).

3.2.3 Histomorphometrical Analysis of the Implantation Bed Vascularization

At 10 days *post implantationem* the lowest numbers of vessels were found in the group of the ICIE16-Cu (1316 ±774 vessels/mm^2), while higher numbers were determined in the groups of

Preprints (www.preprints.org) | NOT PEER-REVIEWED | Posted: 23 May 2022 doi:10.20944/preprints202205.0286.v1

the ICIE16 (2040 ± 1025 vessels/mm^2), of the 45S5 (2643 ± 1331 vessels/mm^2) and the ICIE16-Sr (4012 ± 1791 vessels/mm^2) (Figure 9).

At day 30 post *implantationem* the lowest vessel numbers were still found in the group of the ICIE16-Cu (582.5± 372.9 vessels/mm^2) followed by higher numbers in the groups of the ICIE16-Sr (1806 ± 1548 vessels/mm^2), the ICIE16 (2461 ± 1280 vessels/mm^2) and the 45S5 (2669 ± 985.5 vessels/mm^2) (Figure 9). Thus, a comparable implantation bed vascularization was found at both study time points on all groups (Figure 9).

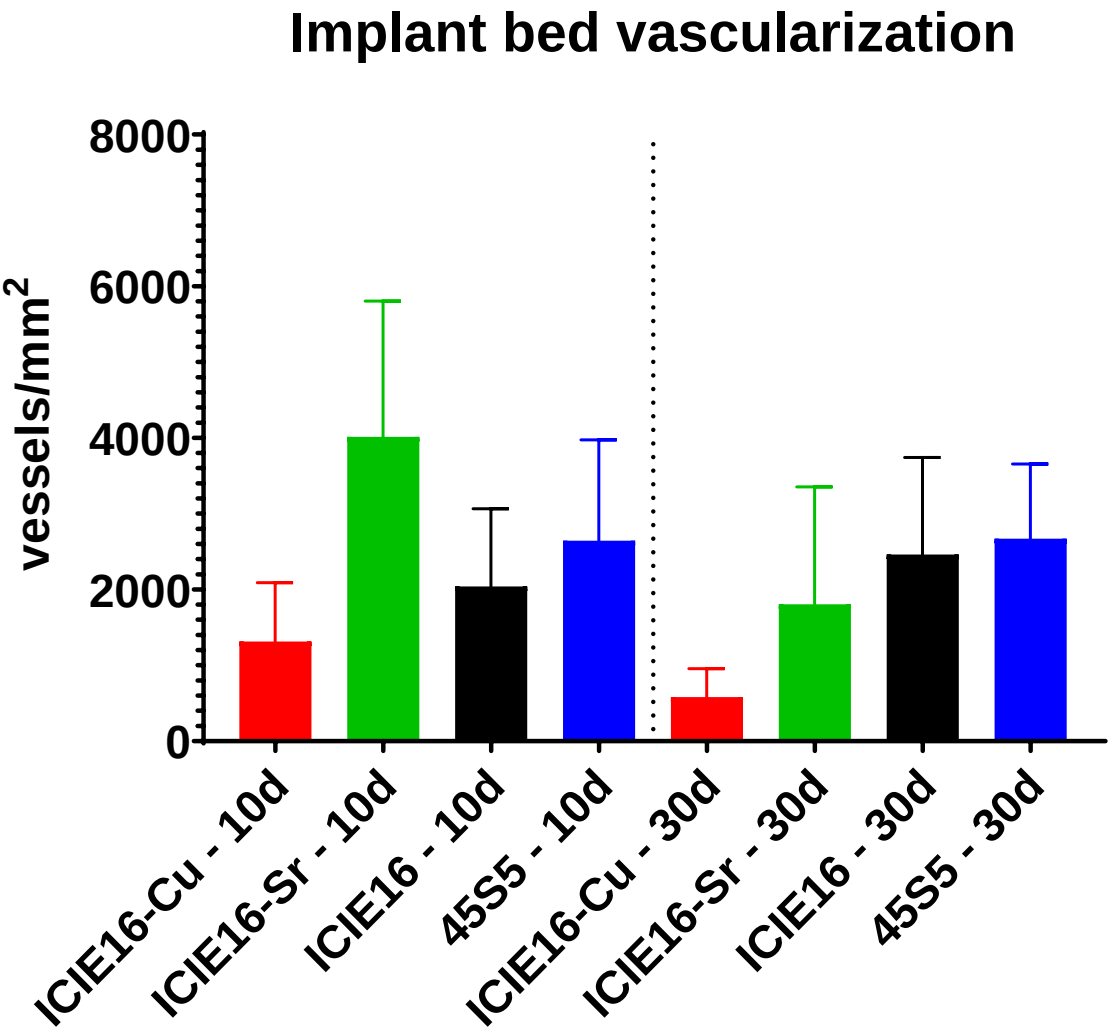

Figure 9. Results of the histomorphometrical analysis of the vessel density (vessel numbers per mm^2) within the implantation beds of the four BG compositions.

4. Discussion

Since its development in the early 70s, bioactive glass has gained increased attention in many different fields in medicine due to its advantages. In the context of bone regeneration, BGs are especially "bioactive" due to the formation of hydroxyapatite on its surface upon making contact with body fluids [13]. This allows the BG implant to bind very well with the host's residual bone, enhancing the integration of the implant [2,32]. In this context, BG has exhibited better integration, due to its binding capacity, than calcium phosphate-based ceramics [2,33]. But more interestingly, BG can be optimally used as drug-delivery material, which can be employed in many fields that include treatment of osteoporotic or traumatic bone defects, radioactive cancer treatment, skin wound healing, etc. [2,4,34–36]. One interesting therapeutic approach is the incorporation of so-called

 doi:10.20944/preprints202205.0286.v1

therapeutic ions [13]. Therapeutic ions can be added in the form of metallic ions that have manifoldly been shown to promote different stimulating effects on a variety of molecular pathways [15–17]. Especially ions such as copper (Cu) and strontium (Sr) have been identified as main actors even in bone regeneration indications [22,24]. Cu^{2+} ions seem to regulate the expression of vascular endothelial growth factor (VEGF), fibronectin, and fibroblastic growth factors (FGFs), which support angiogenesis as an essential component of bone regeneration that allows for migration of relevant cells and prevention of the formation of necrotic implant cores [37]. Copper ions also support osteogenesis as it is a cofactor in the crosslinking of collagen and elastin during bone formation [24]. Another influence of copper ions on bone regeneration is its inhibition of osteoclasts, as a result copper supplementation is used as a treatment of postmenopausal osteoporosis or the augmentation of osteoporotic defects [24]. Additionally, Cu^{2+} ions have revealed to provide an antibacterial potential that can be employed against early local infections [38]. Moreover, Sr^{2+} ions have also shown to influence the bone regeneration process where these ions support Catenin activation [39], expression of Col1, expression of BMP-2, and increase activity of alkaline phosphatase (ALP) [22]. Catenin signalling supports bone matrix formation and regulates differentiation of osteoblasts [40]. An increased ALP activity is a precursor to increased bone formation [41]. Moreover, strontium ions support osteoconductivity of the implants via enhancing their adhesiveness [42], as well as inhibit the formation of osteoclasts which can also be of advantage in augmenting osteoporotic defects [18]. These facts lead to the conclusion that both ions might locally regulate bone cell activities as well as the bone healing process in the course of further remodelling.

In the context of bone tissue regeneration by means of bone substitute materials (BSM), such as calcium phosphate (CaP)- or BG-based materials, it has been observed that the optimal bone substitute has to act as a substrate for bone ingrowth into a defect while being resorbed in the same time frame needed for complete regeneration up to the condition of *restitution ad integrum* [43,44]. Interestingly, it has been shown that nearly all BSM are resorbed via inflammatory pathways [45–48]. In addition to macrophages, multinucleated giant cells (MNGCs) are involved in the tissue reaction to BSM belonging to the cell line of the foreign body giant cells (FBGCs) but are called "biomaterial-associated multinucleated giant cells (BMGCs) as they have been shown to possess both a pro- and also anti-inflammatory phenotype, similar to macrophages [49,50]. They may thus exhibit a substantial influence on the regeneration process. The consensus is that the biomaterial should altogether induce an anti-inflammatory tissue response and thereby also a predominance of M2 macrophages, in order to optimally support tissue regeneration [21]. However, it is completely unknown what influence these so-called therapeutic ions have on inflammatory tissue reactions that are to be strongly connected with tissue regeneration [51]. Thus, it was supposed that their inclusion can be used to control the material-triggered healing process by regulating the induction of M2-macrophages [52,53]. Interestingly, the research in this field starts to understand the immunomodulatory characteristics of different therapeutic ions that have been analysed in previous studies indicating to decrease the migration of macrophages, the formation of BMGCs and fibrous capsules, as well as the detected inflammatory cytokines around the implanted materials [53]. It was concluded that the ion addition might allow to regulate immune responses by altering the ionic microenvironment [54]. The use of therapeutic ions in dental applications, could therefore provide a lot of advantages compared to both purely inorganic bone substitute materials and also to organic biomolecules (*e.g.*, growth factors) such as the lack of risk of decomposition or the possibility to be processed at typical manufacturing conditions [27]. Altogether, it is assumable that the addition of therapeutic ions to bone substitute materials such as BGs might lead to a better bone healing process by adaption of the associated and underlying inflammatory reactions. Thus, the present study was conducted aiming to investigate the chemical and *in vivo* influences of doping ICIE16 BG with strontium and copper ions. Therefore, ICIE16 BG was doped with 5 wt% copper and 5 wt% strontium ions, respectively.

Initially, the examination of the chemical composition of the BGs via EDX analysis revealed that the ion-doped BGs exhibited peaks reflecting the normal element distribution and also the added ions within the respective groups.

 doi:10.20944/preprints202205.0286.v1

To closely observe the release of both therapeutic ions, ICP-OES analysis was conducted. Copper and strontium ions were found to be released from ICIE16-Cu and ICIE16-Sr respectively in an increasing matter over time. Additionally, it was observed that the release of copper ions increased throughout the time points of SBF immersion, while the strontium release reached a steady state between 7 and 15 days. Thereby, the copper-doped materials showed a higher but not significant release at all time points. In this context, it has to be mentioned that both ions belong to the group of the so-called microelements on the basis of their relative abundance in biological cells/tissues and physiological fluids, i.e., concentration > 100 mg/dL and < 100 mg/dL, respectively [55,56]. It has been reported that their high concentrations can be toxic [53,57]. In case of the analysed doped BGs the ion release was found to be in the afore-mentioned concentration window with only one exception in the group of the copper-doped ICIE16-Cu at 14 days. Based on these values it might thus be possible that in this study group an increased inflammatory reaction could be triggered.

The histopathological analysis showed that all BG groups induced moderate foreign body reactions whose manifestation is usually seen in case of a broad variety of bone substitute materials [29,46]. This reaction pattern includes a granulation tissue involving mainly macrophages, BMGCs and lymphocytes, as well as blood vessels normally starting with day 10 post *implantationem*. Signs of (cellular) degradation were observable also beginning with day 10 post *implantationem*, including mononuclear phagocytes crawling within the implant's body and the presence of BMGCs at the material surfaces. Interestingly, the granulation tissue passivated for all ICIE16 groups almost to a slight fibrosis but not in case of the 45S5® BG, which suggests that the 45S5® BG continuously triggers a biodegrading immune reaction. This leads to the conclusion that the ICIE16 BG triggered the observed tissue reaction and undergoes in general a lower cellular biodegradation process compared to that of 45S5® bioglass. Moreover, these results also showed that the added therapeutic ions did not seem to have an influence onto the inflammatory tissue reaction. An answer could be found on basis of the material characteristics of both BG types. Thus, the larger sintering window of ICIE16 BG due to its composition may result in a lower tendency towards crystallization, which could have influenced the tissue reaction on the molecular level [58,59]. In this context it has been described that the initial binding of proteins onto biomaterial surfaces is of high importance for the overall alignment of the following tissue reaction [60]. Thereby, the surface pattern of the biomaterial dictates both (a) the type of proteins bound to the surface and (b) its conformation, which will hereafter expose specific binding sites for different cell receptors and cell types and thus also dictate the foreign body cascade [61]. In this context, it is thinkable that the ICIE16 BG induced a higher expression of Transforming Growth Factor β (TGFβ), especially isoform 1, mainly by macrophages and BMGCs [62]. This finding was already shown by Hernandez-Pando et al., who observed that injected nitrocellulose particles initially caused the BMGCs to express IL-1α, TNFα, and TGFβ [63]. Interestingly, TGFβ was the most persistently expressed cytokine overtime and its expression was associated with extensive chronic fibrosis. An additional explanation for the observed tissue reaction pattern might be found in the fact that the ICIE16 BG contains a considerably lower amount of sodium oxide, while the higher sodium content of the 45S5 BG has shown to induce a strong increase in local pH and is held at least in parts accountable for its dose-dependent cytotoxic effects [64].Thus, it is conceivable that the higher pH value within the implantation bed of the 45S5 BG did not lead to fibrosis but was a trigger for a faster cellular biodegradation and served as an "inductor" of phagocyte accumulation.

Moreover, the histomorphometrical analysis revealed no significant differences between the cell numbers of M1 and M2 macrophages at the different study timepoints - with only one exception for the M1 macrophage numbers in the group of the 4S5S BG only compared to the copper-doped ICIE16-Cu at day 10 *post implantationem*. This finding is indeed also in line with the aforementioned higher phagocyte accumulation in case of 4S5S BG and shows additionally its higher inflammatory potential. Interestingly, the higher M1 macrophage accumulation was only detected at day 10 *post implantationem*, which might be due to fact that the higher pH value in case of 45S5 BG can be restricted to the early phase after implantation. This assumption is based on the fact that is well known that an apatite layer is forming at the surface of the BGs that might prevent former pH value

 doi:10.20944/preprints202205.0286.v1

shifts [13]. This observation might thus be comparable with findings made after implantation of magnesium-based biomaterials [65]. Recent advances in the understanding of corrosion mechanisms have shown that magnesium's susceptibility to corrosion occurs despite the presence of an oxide layer. This film may fail to adequately protect magnesium-based implants in acidic and neutral environments, where it can corrode rapidly exposing the metal underneath to further attack but is has shown to prevent the corrosion process marginally. However, in our case an influence of the copper addition in ICIE16-Cu was not found, as the ratio of M1- and M2-macrophage numbers in this group does not show any significant differences compared to the investigated BG compositions.

Interestingly, another important observation can be extracted from the histomorphometrical data as in nearly every study group – with one exception in the group of the 45S5 BG at day 30 *post implantationem* – as the numbers of pro-inflammatory macrophages tended to be higher. This phenomenon is very interesting even in view of the biocompatibility of the analyzed BGs. Even in case of bone substitute materials it has already been observed that partially higher M1 macrophage numbers were found within their implantation beds, which has been believed to be the "unnatural" immune response to such materials, even in case of natural materials such as collagen membranes amongst others [66,67]. It was also supposed that the occurrence of this pro-inflammatory cell type is associated with the inflammation-based biodegradation pattern [68]. In this context, various studies have revealed a dependency of the biodegradation capacity of macrophages, and oxidative degradation [69]. For example, it was shown that pro-inflammatory macrophages are capable of exerting oxidative stress and release lytic enzymes such as nitric oxide (NO) and reactive oxygen species (ROS) [70,71]. Moreover, high levels of ROS were associated with high expression of pro-inflammatory cytokines in pro-inflammatory macrophages [72]. Furthermore, a study by Wissing et al. demonstrated that LPS/IFN-γ treatment of macrophages led to a pro-inflammatory gene expression profile and induced a significant upregulation of lipid peroxidation, overexpression of the oxidative genes NOX2 and NFκB, and increased enzymatic activity [73]. Thus, the comparable numbers of M1 macrophages in all groups may also hint at comparable biodegradation pattern of the analyzed BG types. Another interesting finding is the localization pattern of the M1- and M2 macrophages found in all study groups. The immunohistochemical detection of anti-inflammatory M2 macrophages revealed that this macrophage subtype remained within the surrounding granulation and connective tissues but not on the surface or within the implant's body. In contrast, pro-inflammatory M1 macrophages appeared on the surface of all implants (and also crawling within) starting from day 10 post *implantationem*. These results suggests that both macrophage subtypes seem to have different functionalities within the foreign body cascade as already suggested [74,75]. Proinflammatory cells seem to engage in cell-mediated resorption, while anti-inflammatory cells seem to be more involved in the regeneration of the surrounding tissue – even in the time frame of the present study. However, no significant differences between the M1 and M2 macrophage subtypes were measured so that it can be concluded that all analyzed biomaterials are biocompatible as they induced in total balanced numbers of M1 and M2 macrophages.

Moreover, and even though copper has been reported to have angiogenetic potential, no significant differences were observed in the histomorphometrical analysis of the implantation bed vascularization. Contradicting to the *in vitro*-based predications of angiogenetic potential of copper, the copper-doped BG ICIE16-Cu but also the strontium-doped material ICIE16-Sr did not enhance implant vascularization in this study.

Altogether, no biological influence of the addition of both of these therapeutic ions onto both the immune response and the vascularization pattern was found. This result is surprising even as both ions have been described to allow influence in both molecular cascades but are in line with another in vivo study including an analysis of silicate-based copper-doping that showed also no influence and more importantly, the materials were observed to hinder the regeneration process [76,77].

However, one limitation of this study was the short-term *in vivo* experiment, that is because bone regeneration occurs on longer time periods and in order to verify the osteogenic potential of these ion-doped bioactive glasses, a further *in vivo* trial using bone implantation models may show another tissue reactivity of the analysed materials – also in view of the bony microenvironment. Another

point to consider is that the investigation of ion-release in SBF can be a precursor to ion-release *in vivo* but it is not exact enough to make accurate conclusion. That is because SBF is different from body fluids in the following points: i) body fluid is a dynamic system while the ion-release measurement was conducted in a static environment, ii) body fluids are "open systems", which means that their components are constantly replaced or renewed whereby SBF was not changed during the analysis timepoints, and iii) SBF does not include all the components of body fluids (*e.g.*, proteins, enzymes, ions, *etc.*). Thus, *in vivo* analysis of the ion release can provide a more accurate concentration within the surrounding tissue and the overall dissolution behaviour.

Another analysis that could provide further understanding is the quantitative measurement of the nanoscale build-up of apatite and whether a correlation could be found with the histomorphometrical results.

Overall, all bioactive glass systems seemed to be biocompatible with an acceptable foreign body reaction that is often seen in case of synthetic bone substitute materials. Finally, and contradicting to published *in vitro* evaluation, copper- and strontium-doping did not significantly influence macrophage polarization, nor vascularization.

Author Contributions: Conceptualization, F.S. and M.B.; methodology, S.N., S.S., O.G., F.S.. and M.B.; software, O.G., F.S. and M.B.; validation, S.A., F.S.. and M.B.; formal analysis, A.M., M.R., S.N., S.S., F.S. and M.B.; investigation, S.A., A.M., Y.R., B.C., O.G., F.S. and M.B.; resources, S.N., S.S., O.G., F.S.. and M.B.; data curation, S.N., S.S., M.R., O.G., F.S.. and M.B.; writing—original draft preparation, S.A., S.N., S.S., O.G., F.S.. and M.B.; writing—review and editing, S.A., S.N., F.S.. and M.B.; visualization, S.A., F.S.. and M.B.; supervision, S.N., F.S.. and M.B.; project administration, S.N., F.S.. and M.B.; funding acquisition, M.B. All authors have read and agreed to the published version of the manuscript.

Funding: This research received no external funding.

Institutional Review Board Statement: The *in vivo* experiments on animals were authorized by the Local Ethical Committee of the Faculty of Medicine (University of Niš, Serbia) based on the approval of the Veterinary Directorate of the Ministry of Agriculture, Forestry and Water Management of the Republic of Serbia (approval number 323-07-01762/2019-05/9; date of approval: 01 March 2019).

Conflicts of Interest: The authors declare no conflict of interest.

References

1. Perić Kačarević, Ž.; Rider, P.; Alkildani, S.; Retnasingh, S.; Pejakić, M.; Schnettler, R.; Gosau, M.; Smeets, R.; Jung, O.; Barbeck, M. An introduction to bone tissue engineering. *Int. J. Artif. Organs* **2020**, *43*, 69–86, doi:10.1177/0391398819876286.
2. Ribas, R.G.; Schatkoski, V.M.; Montanheiro, T.L. do A.; de Menezes, B.R.C.; Stegemann, C.; Leite, D.M.G.; Thim, G.P. Current advances in bone tissue engineering concerning ceramic and bioglass scaffolds: A review. *Ceram. Int.* **2019**, *45*, 21051–21061, doi:10.1016/j.ceramint.2019.07.096.
3. Chacko, N.L.; Abraham, S.; Rao, H.N.S.; Sridhar, N.; Moon, N.; Barde, D.H. A Clinical and Radiographic Evaluation of Periodontal Regenerative Potential of PerioGlas®: A Synthetic, Resorbable Material in Treating Periodontal Infrabony Defects. *J. Int. oral Heal. JIOH* **2014**, *6*, 20–6.
4. Blayney, A.W.; Bebear, J.P.; Williams, K.R.; Portman, M. Ceravital in ossiculoplasty: experimental studies and early clinical results. *J. Laryngol. Otol.* **1986**, *100*, 1359–1366, doi:10.1017/S0022215100101148.
5. Strunz, V.; Bunte, M.; Sauer, G. [Tooth roots made of Ceravital. 1 year's clinical results with a bioactive implantation material]. *Dtsch. Zahnarztl. Z.* **1977**, *32*, 903–904.
6. Chitra, S.; Bargavi, P.; Durgalakshmi, D.; Rajashree, P.; Balakumar, S. Role of sintering temperature dependent crystallization of bioactive glasses on erythrocyte and cytocompatibility. *Process. Appl. Ceram.* **2019**, *13*, 12–23, doi:10.2298/PAC1901012C.
7. Lefebvre, L.; Gremillard, L.; Chevalier, J.; Zenati, R.; Bernache-Assolant, D. Sintering behaviour of 45S5 bioactive glass. *Acta Biomater.* **2008**, *4*, 1894–1903, doi:10.1016/J.ACTBIO.2008.05.019.
8. Stähli, C.; James-Bhasin, M.; Hoppe, A.; Boccaccini, A.R.; Nazhat, S.N. Effect of ion release from Cu-doped 45S5 Bioglass® on 3D endothelial cell morphogenesis. *Acta Biomater.* **2015**, *19*, 15–22, doi:10.1016/j.actbio.2015.03.009.

9. Ciraldo, F.E.; Boccardi, E.; Melli, V.; Westhauser, F.; Boccaccini, A.R. Tackling bioactive glass excessive in vitro bioreactivity: Preconditioning approaches for cell culture tests. *Acta Biomater.* **2018**, *75*, 3–10, doi:10.1016/J.ACTBIO.2018.05.019.
10. Elgayar, I.; Aliev, A.E.; Boccaccini, A.R.; Hill, R.G. Structural analysis of bioactive glasses. *J. Non. Cryst. Solids* **2005**, *351*, 173–183, doi:10.1016/J.JNONCRYSOL.2004.07.067.
11. Hmood, F.; Goerke, O.; Schmidt, F. Chemical Composition Refining of Bioactive Glass for Better Processing Features, Part i. *Biomed. Glas.* **2018**, *4*, 82–94, doi:10.1515/BGLASS-2018-0008/MACHINEREADABLECITATION/RIS.
12. Westhauser, F.; Hohenbild, F.; Arango-Ospina, M.; Schmitz, S.I.; Wilkesmann, S.; Hupa, L.; Moghaddam, A.; Boccaccini, A.R. Bioactive Glass (BG) ICIE16 Shows Promising Osteogenic Properties Compared to Crystallized 45S5-BG. *Int. J. Mol. Sci.* **2020**, *21*, doi:10.3390/IJMS21051639.
13. Baino, F.; Hamzehlou, S.; Kargozar, S. Bioactive glasses: Where are we and where are we going? *J. Funct. Biomater.* **2018**, *9*, doi:10.3390/jfb9010025.
14. Hohenbild, F.; Ospina, M.A.; Schmitz, S.I.; Moghaddam, A.; Boccaccini, A.R.; Westhauser, F. An In Vitro Evaluation of the Biological and Osteogenic Properties of Magnesium-Doped Bioactive Glasses for Application in Bone Tissue Engineering. *Int. J. Mol. Sci.* **2021**, *22*, doi:10.3390/IJMS222312703.
15. Nandi, S.K.; Mahato, A.; Kundu, B.; PrasenjitMukherjee Doped Bioactive Glass Materials in Bone Regeneration. *Adv. Tech. Bone Regen.* **2016**, doi:10.5772/63266.
16. Goh, Y.F.; Alshemary, A.Z.; Akram, M.; Abdul Kadir, M.R.; Hussain, R. Bioactive Glass: An In-Vitro Comparative Study of Doping with Nanoscale Copper and Silver Particles. *Int. J. Appl. Glas. Sci.* **2014**, *5*, 255–266, doi:10.1111/ijag.12061.
17. Opitz, P.; Besch, L.; Panthöfer, M.; Kabelitz, A.; Unger, R.E.; Emmerling, F.; Mondeshki, M.; Tremel, W. Insights into the In Vitro Formation of Apatite from Mg-Stabilized Amorphous Calcium Carbonate. *Adv. Funct. Mater.* **2021**, *31*, 2007830, doi:10.1002/ADFM.202007830.
18. Glenske, K.; Donkiewicz, P.; Kowitsch, A.; Milosevic-Oljaca, N.; Rider, P.; Rofall, S.; Franke, J.; Jung, O.; Smeets, R.; Schnettler, R.; et al. Applications of Metals for Bone Regeneration. *Int J Mol Sci* **2018**, *19*, doi:10.3390/ijms19030826.
19. El-Rashidy, A.A.; Roether, J.A.; Harhaus, L.; Kneser, U.; Boccaccini, A.R. Regenerating bone with bioactive glass scaffolds: A review of in vivo studies in bone defect models. *Acta Biomater.* **2017**, *62*, 1–28, doi:10.1016/J.ACTBIO.2017.08.030.
20. Anderson, J.M.; Rodriguez, A.; Chang, D.T. Foreign body reaction to biomaterials. *Semin Immunol* **2008**, *20*, 86–100, doi:10.1016/j.smim.2007.11.004.
21. Sridharan, R.; Cameron, A.R.; Kelly, D.J.; Kearney, C.J.; O'Brien, F.J. Biomaterial based modulation of macrophage polarization: a review and suggested design principles. *Mater. Today* **2015**, *18*, 313–325, doi:10.1016/J.MATTOD.2015.01.019.
22. Nardone, V.; Zonefrati, R.; Mavilia, C.; Romagnoli, C.; Ciuffi, S.; Fabbri, S.; Palmini, G.; Galli, G.; Tanini, A.; Brandi, M.L. In Vitro Effects of Strontium on Proliferation and Osteoinduction of Human Preadipocytes. *Stem Cells Int.* **2015**, *2015*, doi:10.1155/2015/871863.
23. Rossi, L.M.M.; Copes, R.M.; Dal Osto, L.C.; Flores, C.; Comim, F.V.; Premaor, M.O. Factors related with osteoporosis treatment in postmenopausal women. *Medicine (Baltimore).* **2018**, *97*, doi:10.1097/MD.0000000000011524.
24. Lowe, N.M.; Fraser, W.D.; Jackson, M.J. Is there a potential therapeutic value of copper and zinc for osteoporosis? *Proc. Nutr. Soc.* **2002**, *61*, 181–185, doi:10.1079/pns2002154.
25. Weng, L.; Boda, S.K.; Teusink, M.J.; Shuler, F.D.; Li, X.; Xie, J. Binary Doping of Strontium and Copper Enhancing Osteogenesis and Angiogenesis of Bioactive Glass Nanofibers while Suppressing Osteoclast Activity. *ACS Appl. Mater. Interfaces* **2017**, *9*, 24484–24496, doi:10.1021/acsami.7b06521.
26. Malachová, K.; Praus, P.; Rybková, Z.; Kozák, O. Antibacterial and antifungal activities of silver, copper and zinc montmorillonites. *Appl. Clay Sci.* **2011**, *53*, 642–645, doi:10.1016/J.CLAY.2011.05.016.
27. Rebouças, J. de S.; Santos-Magalhães, N.S.; Formiga, F.R. Cardiac Regeneration using Growth Factors: Advances andChallenges. *Arq. Bras. Cardiol.* **2016**, *107*, 271, doi:10.5935/ABC.20160097.
28. Lindner, C.; Pröhl, A..; Abels, M.; Löffler, T.; Batinic, M.; Jung, O.; Barbeck, M. *Specialized Histological and Histomorphometrical Analytical Methods for Biocompatibility Testing of Biomaterials for Maxillofacial Surgery in (Pre-) Clinical Studies*; International Institute of Anticancer Research, 2020; Vol. 34, pp. 3137–3152;.

29. Abels, M.; Alkildani, S.; Pröhl, A.; Xiong, X.; Krastev, R.; Korzinskas, T.; Stojanovic, S.; Jung, O.; Najman, S.; Barbeck, M. The Granule Size Mediates the In Vivo Foreign Body Response and the Integration Behavior of Bone Substitutes. *Materials (Basel).* **2021**, *14*, 7372, doi:10.3390/ma14237372.
30. Hmood, F.J.; Schmidt, F.; Goerke, O.; Günster, J. Investigation of chemically modified ICIE16 bioactive glass, Part II. *J. Ceram. Sci. Technol.* **2020**, *11*, 1–9, doi:10.4416/JCST2019-00031.
31. Kokubo, T.; Takadama, H. How useful is SBF in predicting in vivo bone bioactivity? *Biomaterials* **2006**, *27*, 2907–2915, doi:10.1016/J.BIOMATERIALS.2006.01.017.
32. Fu, Q.; Saiz, E.; Rahaman, M.N.; Tomsia, A.P. Bioactive glass scaffolds for bone tissue engineering: state of the art and future perspectives. *Mater. Sci. Eng. C* **2011**, *31*, 1245–1256, doi:10.1016/J.MSEC.2011.04.022.
33. Fu, Q.; Saiz, E.; Rahaman, M.N.; Tomsia, A.P. Toward strong and tough glass and ceramic scaffolds for bone repair. *Adv. Funct. Mater.* **2013**, *23*, 5461–5476, doi:10.1002/adfm.201301121.
34. Wu, C.; Chang, J. Multifunctional mesoporous bioactive glasses for effective delivery of therapeutic ions and drug/growth factors. *J. Control. Release* **2014**, *193*, 282–295, doi:10.1016/J.JCONREL.2014.04.026.
35. Baino, F.; Fiume, E.; Ciavattini, S.; Kargozar, S.; Borges, R.; Genova, L.A.; Marchi, J.; Verné, E. Biomedical Radioactive Glasses for Brachytherapy. *Mater. (Basel, Switzerland)* **2021**, *14*, 1–18, doi:10.3390/MA14051131.
36. Hu, H.; Tang, Y.; Pang, L.; Lin, C.; Huang, W.; Wang, D.; Jia, W. Angiogenesis and Full-Thickness Wound Healing Efficiency of a Copper-Doped Borate Bioactive Glass/Poly(lactic-co-glycolic acid) Dressing Loaded with Vitamin E in Vivo and in Vitro. *ACS Appl. Mater. Interfaces* **2018**, *10*, 22939–22950, doi:10.1021/acsami.8b04903.
37. Rider, P.; Kačarević, Ž.P.; Alkildani, S.; Retnasingh, S.; Schnettler, R.; Barbeck, M. *Additive manufacturing for guided bone regeneration: A perspective for alveolar ridge augmentation*; **2018**; Vol. 19; ISBN 4930206073.
38. Wu, C.; Zhou, Y.; Xu, M.; Han, P.; Chen, L.; Chang, J.; Xiao, Y. Copper-containing mesoporous bioactive glass scaffolds with multifunctional properties of angiogenesis capacity, osteostimulation and antibacterial activity. *Biomaterials* **2013**, *34*, 422–433, doi:10.1016/J.BIOMATERIALS.2012.09.066.
39. Yang, F.; Yang, D.; Tu, J.; Zheng, Q.; Cai, L.; Wang, L. Strontium enhances osteogenic differentiation of mesenchymal stem cells and in vivo bone formation by activating Wnt/catenin signaling. *Stem Cells* **2011**, *29*, 981–991, doi:10.1002/stem.646.
40. Chen, Y.; Whetstone, H.C.; Lin, A.C.; Nadesan, P.; Wei, Q.; Poon, R.; Alman, B.A. Beta-catenin signaling plays a disparate role in different phases of fracture repair: implications for therapy to improve bone healing. *PLoS Med.* **2007**, *4*, 1216–1229, doi:10.1371/JOURNAL.PMED.0040249.
41. Prins, H.J.; Braat, A.K.; Gawlitta, D.; Dhert, W.J.A.; Egan, D.A.; Tijssen-Slump, E.; Yuan, H.; Coffer, P.J.; Rozemuller, H.; Martens, A.C. In vitro induction of alkaline phosphatase levels predicts in vivo bone forming capacity of human bone marrow stromal cells. *Stem Cell Res.* **2014**, *12*, 428–440, doi:10.1016/j.scr.2013.12.001.
42. Liu, C.; Zhang, Y.; Wang, L.; Zhang, X.; Chen, Q.; Wu, B. A Strontium-Modified Titanium Surface Produced by a New Method and Its Biocompatibility In Vitro. *PLoS One* **2015**, *10*, e0140669, doi:10.1371/JOURNAL.PONE.0140669.
43. Kübler, N.R. [Osteoinduction and -reparation]. *Mund. Kiefer. Gesichtschir.* **1997**, *1*, 2–25, doi:10.1007/BF03043502.
44. Goldberg, V.M.; Stevenson, S. The biology of bone grafts. *Semin. Arthroplasty* **1993**, *4*, 58–63.
45. Zhao, R.; Yang, R.; Cooper, P.R.; Khurshid, Z.; Shavandi, A.; Ratnayake, J. Bone Grafts and Substitutes in Dentistry: A Review of Current Trends and Developments. *Molecules* **2021**, *26*, doi:10.3390/MOLECULES26103007.
46. Pröhl, A.; Batinic, M.; Alkildani, S.; Hahn, M.; Radenkovic, M.; Najman, S.; Jung, O.; Barbeck, M. In vivo analysis of the biocompatibility and bone healing capacity of a novel bone grafting material combined with hyaluronic acid. *Int. J. Mol. Sci.* **2021**, *22*, doi:10.3390/ijms22094818.
47. Conserva, E.; Foschi, F.; Cancedda, R.; Mastrogiacomo, M. In vitro and in vivo osteoinductive and osteoconductive properties of a synthetic bone substitute. *Int. J. Oral Maxillofac. Implants* **2013**, *28*, e432–e439, doi:10.11607/JOMI.TE23.
48. Solakoglu, Ö.; Götz, W.; Heydecke, G.; Schwarzenbach, H. Histological and immunohistochemical comparison of two different allogeneic bone grafting materials for alveolar ridge reconstruction: A prospective randomized trial in humans. *Clin. Implant Dent. Relat. Res.* **2019**, *21*, 1002–1016, doi:10.1111/CID.12824.
49. Anderson, J.M. Multinucleated giant cells. *Curr Opin Hematol.* **2000**, doi: 10.1097/00062752-200001000-00008.

50. Miron, R.J.; Bosshardt, D.D. Multinucleated Giant Cells: Good Guys or Bad Guys? *Tissue Eng Part B Rev* **2018**, *24*, 53–65, doi:10.1089/ten.TEB.2017.0242.
51. O'Neill, E.; Awale, G.; Daneshmandi, L.; Umerah, O.; Lo, K.W.H. The roles of ions on bone regeneration. *Drug Discov. Today* **2018**, *23*, 879–890, doi:10.1016/J.DRUDIS.2018.01.049.
52. Berthon, G. Is copper pro- or anti-inflammatory? A reconciling view and a novel approach for the use of copper in the control of inflammation. *Agents Actions* **1993**, *39*, 210–217, doi:10.1007/BF01998975.
53. Díez-Tercero, L.; Delgado, L.M.; Bosch-Rué, E.; Perez, R.A. Evaluation of the immunomodulatory effects of cobalt, copper and magnesium ions in a pro inflammatory environment. *Sci. Reports 2021 111* **2021**, *11*, 1–13, doi:10.1038/s41598-021-91070-0.
54. Batool, F.; Özçelik, H.; Stutz, C.; Gegout, P.Y.; Benkirane-Jessel, N.; Petit, C.; Huck, O. Modulation of immune-inflammatory responses through surface modifications of biomaterials to promote bone healing and regeneration. *J. Tissue Eng.* **2021**, *12*, doi:10.1177/20417314211041428.
55. Somarouthu, S.; Ohh, J.; Shaked, J.; Cunico, R.L.; Yakatan, G.; Corritori, S.; Tami, J.; Foehr, E.D. Quantitative bioanalysis of strontium in human serum by inductively coupled plasma-mass spectrometry. *Futur. Sci. OA* **2015**, *1*, doi:10.4155/FSO.15.76.
56. Kubala-Kukuś, A.; Banaś, D.; Braziewicz, J.; Majewska, U.; Pajek, M.; Wudarczyk-Moćko, J.; Antczak, G.; Borkowska, B.; Góźdź, S.; Smok-Kalwat, J. Analysis of Copper Concentration in Human Serum by Application of Total Reflection X-ray Fluorescence Method. *Biol. Trace Elem. Res.* **2014**, *158*, 22, doi:10.1007/S12011-013-9884-4.
57. Cortizo, M.C.; De Mele, M.F.L. Cytotoxicity of copper ions released from metal: variation with the exposure period and concentration gradients. *Biol. Trace Elem. Res.* **2004**, *102*, 129–141, doi:10.1385/BTER:102:1-3:129.
58. Peric Kacarevic, Z.; Kavehei, F.; Houshmand, A.; Franke, J.; Smeets, R.; Rimashevskiy, D.; Wenisch, S.; Schnettler, R.; Jung, O.; Barbeck, M. Purification processes of xenogeneic bone substitutes and their impact on tissue reactions and regeneration. *Int J Artif Organs* **2018**, 391398818771530, doi:10.1177/0391398818771530.
59. Boccaccini, A.R.; Chen, Q.; Lefebvre, L.; Gremillard, L.; Chevalier, J. Sintering, crystallisation and biodegradation behaviour of Bioglass®-derived glass-ceramics. *Faraday Discuss.* **2007**, *136*, 27–44, doi:10.1039/b616539g.
60. Luttikhuizen, D.T.; Harmsen, M.C.; Van Luyn, M.J. Cellular and molecular dynamics in the foreign body reaction. *Tissue Eng* **2006**, *12*, 1955–1970, doi:10.1089/ten.2006.12.1955.
61. Lee, J.; Byun, H.; Perikamana, S.K.M.; Lee, S.; Shin, H.; Madhurakkat Perikamana, S.K.; Lee, S.; Shin, H.; Hayeon, B. Current Advances in Immunomodulatory Biomaterials for Bone Regeneration. *Adv. Healthc. Mater.* **2019**, *8*, 1–20, doi:10.1002/adhm.201801106.
62. Lari, R.; Fleetwood, A.J.; Kitchener, P.D.; Cook, A.D.; Pavasovic, D.; Hertzog, P.J.; Hamilton, J.A. Macrophage lineage phenotypes and osteoclastogenesis—Complexity in the control by GM-CSF and TGF-β. *Bone* **2007**, *40*, 323–336, doi:10.1016/J.BONE.2006.09.003.
63. Hernandez-Pando, R.; Bornstein, Q.L.; Leon, D.A.; Orozco, E.H.; Madrigal, V.K.; Cordero, E.M.; Aguilar Leon, D.; Orozco, E.H.; Madrigal, V.K.; Martinez Cordero, E. Inflammatory cytokine production by immunological and foreign body multinucleated giant cells. *Immunology* **2000**, *100*, 352–358, doi:10.1046/j.1365-2567.2000.00025.x.
64. Rizwan, M.; Hamdi, M.; Basirun, W.J. Bioglass® 45S5-based composites for bone tissue engineering and functional applications. *J. Biomed. Mater. Res. A* **2017**, *105*, 3197–3223, doi:10.1002/JBM.A.36156.
65. Jung, O.; Hesse, B.; Stojanovic, S.; Seim, C.; Weitkamp, T.; Batinic, M.; Goerke, O.; Kačarević, Ž.P.; Rider, P.; Najman, S.; et al. Biocompatibility Analyses of HF-Passivated Magnesium Screws for Guided Bone Regeneration (GBR). *Int. J. Mol. Sci.* **2021**, *22*, doi:10.3390/IJMS222212567.
66. Kapogianni, E.; Alkildani, S.; Radenkovic, M.; Xiong, X.; Krastev, R.; Stöwe, I.; Bielenstein, J.; Jung, O.; Najman, S.; Barbeck, M.; et al. The early fragmentation of a bovine dermis-derived collagen barrier membrane contributes to transmembraneous vascularization—A possible paradigm shift for guided bone regeneration. *Membranes (Basel).* **2021**, *11*, doi:10.3390/membranes11030185.
67. Radenković, M.; Alkildani, S.; Stoewe, I.; Bielenstein, J.; Sundag, B.; Bellmann, O.; Jung, O.; Najman, S.; Stojanović, S.; Barbeck, M. Comparative in vivo analysis of the integration behavior and immune response of collagen-based dental barrier membranes for guided bone regeneration (Gbr). *Membranes (Basel).* **2021**, *11*, doi:10.3390/membranes11090712.

68. Yunna, C.; Mengru, H.; Lei, W.; Weidong, C. Macrophage M1/M2 polarization. *Eur. J. Pharmacol.* **2020**, *877*, 173090, doi:10.1016/J.EJPHAR.2020.173090.
69. Virág, L.; Jaén, R.I.; Regdon, Z.; Boscá, L.; Prieto, P. Self-defense of macrophages against oxidative injury: Fighting for their own survival. *Redox Biol.* **2019**, *26*, 101261, doi:10.1016/J.REDOX.2019.101261.
70. Groemping, Y.; Lapouge, K.; Smerdon, S.J.; Rittinger, K. Molecular basis of phosphorylation-induced activation of the NADPH oxidase. *Cell* **2003**, *113*, 343–355, doi:10.1016/S0092-8674(03)00314-3.
71. Tan, H.Y.; Wang, N.; Li, S.; Hong, M.; Wang, X.; Feng, Y. The Reactive Oxygen Species in Macrophage Polarization: Reflecting Its Dual Role in Progression and Treatment of Human Diseases. *Oxid. Med. Cell. Longev.* **2016**, *2016*, doi:10.1155/2016/2795090.
72. Song, M.G.; Ryoo, I.G.; Choi, H.Y.; Choi, B.H.; Kim, S.T.; Heo, T.H.; Lee, J.Y.; Park, P.H.; Kwak, M.K. NRF2 Signaling Negatively Regulates Phorbol-12-Myristate-13-Acetate (PMA)-Induced Differentiation of Human Monocytic U937 Cells into Pro-Inflammatory Macrophages. *PLoS One* **2015**, *10*, doi:10.1371/JOURNAL.PONE.0134235.
73. Wissing, T.B.; Bonito, V.; van Haaften, E.E.; Doeselaar, M. van; Brugmans, M.M.; Janssen, H.M.; Bouten, C. V.; Smits, A.I. Macrophage-driven biomaterial degradation depends on scaffold microarchitecture. *Front. Bioeng. Biotechnol.* **2019**, *7*, 87, doi:10.3389/FBIOE.2019.00087/BIBTEX.
74. Jamalpoor, Z.; Asgari, A.; Lashkari, M.H.; Mirshafiey, A.; Mohsenzadegan, M. Modulation of macrophage polarization for bone tissue engineering applications. *Iran. J. Allergy, Asthma Immunol.* **2018**, *17*, 398–408, doi:10.18502/ijaai.v17i5.298.
75. Barbeck, M.; Schröder, M.L.; Alkildani, S.; Jung, O.; Unger, R.E. Exploring the biomaterial-induced secretome: Physical bone substitute characteristics influence the cytokine expression of macrophages. *Int. J. Mol. Sci.* **2021**, *22*, 1–21, doi:10.3390/ijms22094442.
76. Lin, Y.; Xiao, W.; Bal, B.S.; Rahaman, M.N. Effect of copper-doped silicate 13-93 bioactive glass scaffolds on the response of MC3T3-E1 cells in vitro and on bone regeneration and angiogenesis in rat calvarial defects in vivo. *Mater. Sci. Eng. C* **2016**, *67*, 440–452, doi:10.1016/j.msec.2016.05.073.
77. Bührer, G.; Rottensteiner, U.; Hoppe, A.; Detsch, R.; Dafinova, D.; Fey, T.; Greil, P.; Weis, C.; Beier, J.P.; Boccacini, A.R.; et al. Evaluation of in vivo angiogenetic effects of copper doped bioactive glass scaffolds in the AV loop model. *Biomed. Glas.* **2016**, *2*, 111–117, doi:10.1515/bglass-2016-0013.